Title: **Error Propagation for Velocity and Shear Stress Prediction Using 2D Models For Environmental Management**

Authors:

Gregory B. Pasternack[1]*, Andrew T. Gilbert[1], Joseph M. Wheaton[1,2], Evan M. Buckland[1]

Addresses:

[1]Department of Land, Air, and Water Resources, University of California, One Shields Avenue, Davis, CA 95616-8626, USA;

[2]Institute of Geography and Earth Sciences, University of Wales, Aberystwyth, Llandinam Building, Penglais Campus, Aberystwyth, Ceredigion SY23 3DB, Wales, UK

Keywords: shear stress, 2D models, river restoration, hydraulics

Cite as: **Pasternack, G. B., Gilbert, A. T., Wheaton, J. M., Buckland, E. M. 2006. Error Propagation for Velocity and Shear Stress Prediction Using 2D Models For Environmental Management. Journal of Hydrology 328:227-241. DOI: 10.1016/j.jhydrol.2005.12.003.**

https://www.sciencedirect.com/science/article/pii/S0022169405006657

Accepted

ABSTRACT

Resource managers, scientists, government regulators, and stakeholders are considering sophisticated numerical models for managing complex environmental problems. In this study, observations from a river-rehabilitation experiment involving gravel augmentation and spawning habitat enhancement were used to assess sources and magnitudes of error in depth, velocity, and shear velocity predictions made at the 1-m scale with a commercial 2-dimensional (depth-averaged) model. Error in 2D model depth prediction averaged 21%. This error was attributable to topographic survey resolution, which at 1 pt per 1.14 m^2, was inadequate to resolve small humps and depressions influencing point measurements. Error in 2D model velocity prediction averaged 29%. More than half of this error was attributable to depth prediction error. Despite depth and velocity error, 56% of tested 2D model predictions of shear velocity were within the 95 % confidence limit of the best field-based estimation method. Ninety percent of the error in shear velocity prediction was explained by velocity prediction error. Multiple field-based estimates of shear velocity differed by up to 160%, so the lower error for the 2D model's predictions suggests such models are at least as accurate as field measurement. 2D models enable detailed, spatially distributed estimates compared to the small number measurable in a field campaign of comparable cost. They also can be used for design evaluation. Although such numerical models are limited to channel types adhering to model assumptions and yield predictions only accurate to ~20-30%, they can provide a useful tool for river rehabilitation design and assessment, including spatially diverse habitat heterogeneity as well as for pre- and post-project appraisal.

Accepted

1 1. INTRODUCTION

2

3 Two-dimensional hydrodynamic numerical (2D) models are now widely available at low
4 cost and are being used in environmental science and management. Many previous studies have
5 tested the spread in model predictions to variability in initial and boundary conditions
6 (contingency analysis) , parameter values (sensitivity analysis), wetting and drying schemes, and
7 mesh discretization (e.g. Bates and Anderson, 1996; Tchamen and Kahawita, 1998; Hardy et al.,
8 1999; Byrd and Furbish, 2000; French and Clifford, 2000). Some studies have used 2D models
9 as a surrogate for large-scale manipulative experimentation that is impractical or disallowed in
10 nature (Miller, 1995; Cao et al., 2003). Others have used 2D models for investigating
11 geomorphic processes (e.g. Miller and Cluer, 1998; Nicholas and Walling, 1998; Rathburn and
12 Wohl, 2003), flood inundation (Bates et al., 1992; Stewart et al., 1999), water quality and soil
13 contamination (Moulin and Ben Slama, 1998; Stewart et al., 1998), and aquatic microhabitat
14 quality (Leclerc, 1995; Ghamen et al., 1996; Tiffan et al., 2002). Beyond characterizing existing
15 conditions, 2D models are now even being used to aid design and evaluation of river
16 rehabilitation projects in regulated gravel-bed rivers (Pasternack et al., 1994; Wheaton et al.,
17 2004 A,B). In these cases, model limitations are recognized and valued.
18 While all management tools have residual uncertainty that can never be eliminated, there
19 are sources of quantifiable error whose constraint would boost confidence in the practical
20 application of 2D models among a sometimes skeptical audience of academic scientists, resource
21 managers, government regulators, and private consultants who are being confronted with such
22 models with increasing frequency. One large source of uncertainty is model validation. Similar
23 to the advancement from lumped to distributed hydrological models, changing from 1D to 2D

Accepted

hydrodynamic models should increase the breadth of model validation needed.

Previous environmental applications have used either cross-section or point-based measurements of downstream-directed flow components to determine depth and velocity prediction deviation from observations, often with little to no analysis of causes of error (e.g. Rathburn, 2001; Gard, 2003; Pasternack et al., 2004; Gard, 2005). Although flood inundation area can be validated using aerial photos or Synthetic Aperture Radar satellite imagery as a large-scale surrogate for the 2D depth pattern (Bates and De Roo, 2000), analogous approaches for validating large-scale 2D velocity pattern are lacking. Qualitative surface velocity-vector patterns may be observed using floating ropes or buoys that trace 2D particle paths as well as hand-sketches or movies of flow pattern. However, such approaches cannot identify subaqueous 2-layer velocity patterns.

To assess point-scale velocity vectors through depth in wadable gravel-bedded reaches, 2D or 3D sensors may be used (e.g. Rhoads and Kenworthy, 1995; Biron et al., 1998; Lane and Richards, 1998; Nicholas and Sambrook Smith, 1999). This approach is highly time-consuming and expensive. It is challenging to accurately record multiple flow components through depth over a ~10^4 m^2 area, while accurately referencing measurement direction to the 2D model's coordinate system, and impossible to do so simultaneously (Booker et al., 2001). Furthermore, it is unclear how to scale-up 0.5 mm point measurements to compare against averages over ~0.5-3 m^2 model cells. Also, moving 3D sensor data into a 2D model can introduce error through averaging methods. Attempts are being made to use boat-based 3D velocity profilers coupled to RTK GPS units for water depths > 2 m (e.g. Shields et al., 2003), but this approach also averages over variable spatial scales that do not match the 2D-model computational scale and does not resolve the log-linear vertical velocity profile.

Accepted

For regulated, gravel-bed river management, there is a need to predict sediment entrainment, which adds more error through the propagation of potentially inaccurate depth and velocity predictions through additional equations as well as the error inherent in shear velocity equations (Lane et al., 1999). Because gravel-bed rivers have a lower ratio of water depth to grain size than sand-bed rivers, they have more complex fluid mechanics and sediment transport boundary regimes. By definition, 2D models cannot produce vertical velocity gradients in lateral or downstream directions or produce up- and down-welling, all of which are important contributors to drag and lift forces responsible for grain entrainment (Nelson et al., 2001). Also, they do not represent hyporheic flow mechanics responsible for grain vibrations and possible ejections from the bed.

These deterministic limitations raise a serious challenge to the suitability of 2D models for use in sediment entrainment prediction. Are the "lumped" physics in 2D models sufficient to produce predictions at least as accurate as standard field-measurement methods and better than widely used 1D models? Through a detailed evaluation of the performance of 2D models in matching observed point velocity measurements, Lane et al. (1999) found that optimization of the bed roughness parameter within realistic limits yielded highly accurate estimates of downstream velocity, a primary variable governing sediment entrainment.

Despite this, Lane et al. (1999) proposed that 2D models be abandoned in favor of 3D models for predicting fluid dynamics and associated processes in gravel bed rivers. 3D models ought to be superior given their more detailed representation of physics, and they do provide more accurate predictions of the lateral velocity component. However, depending on the particular environmental management application, 2D models may be more appropriate than 3D models. First, it is presently infeasible to collect 3D velocity data and transform it to calibrate

Accepted

and validate 3D models over $>10^4$ m^2 area. Second, many important geomorphic and ecological functions critical to environmental management have been related to depth-average hydraulics and are yet to be related to 3D fluid dynamics. Third, even where a geomorphic process has been related to 3D fluid dynamics, such as in the case of outer bank erosion in a meander bend, it is unclear which model node's shear stress component should be used to drive the process. Fourth, the number and configuration of secondary circulation cells in 3D models exhibit a sensitive dependence on boundary and initial conditions in some channel configurations, necessitating further basic research. Finally, although 3D models include more physics than 2D models, they too are flawed representations of even more complex sediment entrainment phenomena, and thus involve "lumped" evaluation. The selection of 1D, 2D, or 3D predictive capability should hinge on predictive success relative to field observation for the particular environmental problem at hand, rather than theoretical grounds alone.

Improving the evaluation of depth, velocity, and shear velocity prediction in 2D models is an important basic science need prior to community acceptance or rejection of expanded utilization of 2D models in gravel-bed river management. In this study, 1906 metric tons of gravel were placed in a regulated river as a manipulative river-rehabilitation experiment according to a design that had been iteratively vetted with the aid of a 2D model. The overall question addressed here is whether the 2D model predictions of depth, velocity, and shear velocity used in the rehabilitation design and post-project evaluation process were sufficiently accurate for that purpose. Specific study objectives were to: (1) measure and characterize vertical velocity profiles over the artificially contoured gravel bed, (2) compare observed and 2D-model predicted flow kinematics, including depth, velocity, and total shear velocity, and (3) assess practical methods for estimating bed shear velocity from model-predicted total shear

Accepted

velocity. The conclusions suggest practical means of reducing prediction error for use of 2D models. As a next step beyond previous important contributions in this area (e.g. Lane et al., (1999), this study tests the utility of 2D models for use in regulated-river rehabilitation projects.

2. STUDY SITE

2.1 River Rehabilitation in Central Valley, California

River rehabilitation by gravel augmentation is being implemented in the Central Valley of California, USA in accordance with the CALFED Bay-Delta Program's Ecosystem Restoration Program Draft Stage 1 Implementation Plan to enhance aquatic habitat and rehabilitate fluvial geomorphic processes. Many rehabilitation projects are founded on research demonstrating that salmon-spawning habitat is a primary limiting constraint on fish populations in the Sacramento-San Joaquin river system (Moyle, 1994; Fisher, 1994; Brown, 2000). Access to historic spawning habitat has been blocked by dams (Moyle and Randall, 1998), with remaining downstream habitat suffering from flow regulation and water quality degradation due to adjacent land use (e.g. agriculture, gravel mining, and residential development).

In this study the Spawning Habitat Integrated Rehabilitation Approach (SHIRA) was used to aid experimental design. SHIRA integrates concepts from hydrology, ecology, biology, geomorphology, and engineering to design and evaluate alternative channel configurations for a degraded river (Pasternack et al., 2004; Wheaton et al, 2004 A, B). Central to this approach is testing of predictions made by transparent design hypotheses regarding environmental processes over 10^{-1}-10^{4} m scales. In this SHIRA application, a 2D model aided evaluation of the relative performance of design alternatives and the final as-built experimental configuration down to the

Accepted

0.1-1 m scale that fish are attune to (methodology detailed in Wheaton et al. (2004 B)). Monitoring is used to evaluate SHIRA predictions (Merz and Setka, 2004; Merz and Ochikubo Chan, 2005; Merz et al., 2004; Wheaton et al, 2004 C; Merz et al., In Press) and drive adaptive management. Between 2001-2005 SHIRA was used on the Mokelumne River to manage placement and monitoring of 1633-5214 metric tons of gravel per year.

2.2 2002 Rehabilitation Site

The present study was performed at the 2002 site located on the Lower Mokelumne River ~ 4 km downstream of Camanche Reservoir (Fig. 1a). The 2002 project included topographic feature creation at three spatial scales (Fig. 1b). At the reach scale (10^2 channel widths), gravel was used to meet the river's coarse sediment budget demand, elevate the bed, and increase riffle slopes. At the geomorphic-unit scale (10^1 -10^2 channel widths), flow was routed through a sequence of 3 broad riffles and narrow pools to promote deposition on riffles and scour in pools. At the hydraulic unit scale (10^{-1}-10^0 channel widths), 3 boulder complexes were used to encourage localized scour and create shear-zones, channel constrictions, hydraulic jumps, and standing waves. Also, pool exit slopes at pool-riffle transitions were shaped to promote intragravel flow and encourage flow to diverge across riffles.

3. METHODS

To assess accuracy in 2D model predictions of depth, velocity, and shear velocity under typical post-rehabilitation conditions, field measurements and model predictions were made for the 2002 rehabilitation site for two different kinds of spatially explicit data. To assess spatially coherent lateral variability in depth and velocity associated with 10-m scale pool-riffle structure

Accepted

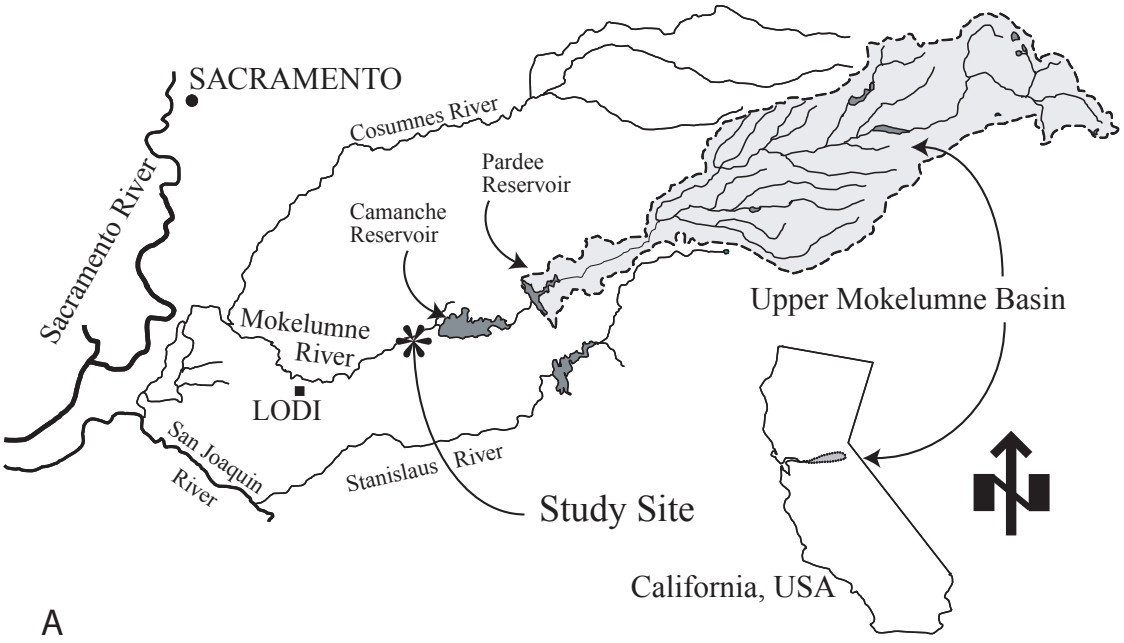
SACRAMENTO
Cosumnes River
Sacramento River
Pardee
Reservoir
Camanche
Reservoir
Mokelumne
River
LODI
San Joaquin
River
Stanislaus River
Study Site
Upper Mokelumne Basin
California, USA
A

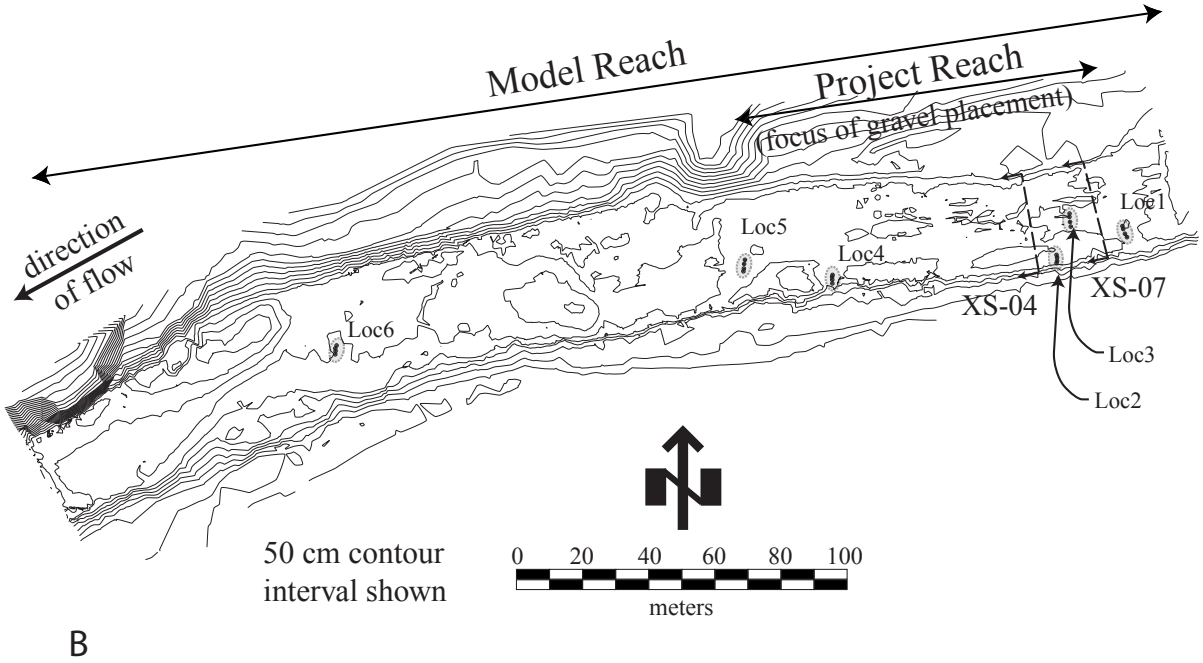
Model Reach
Project Reach
(focus of gravel placement)
direction
of flow
Loc1
Loc5
Loc4
XS-07
XS-04
Loc6
Loc3
Loc2
50 cm contour
interval shown
0 20 40 60 80 100
meters
B

Figure 1

and 1-m scale bed-feature variability, depth and velocity were characterized across along two cross-sections (Fig. 1b) with the same recently placed bed material. The cross-sections happened to be numbered 4 and 7 based on the pre-project model validation experimental design, but only 2 cross-sections were assessed post-project in favour of the second method of validation reported next. To assess variability in depth, velocity, and shear velocity in response to differing point-scale bed material grain size, bed-features, and 2D flow patterns, measurements were made over twenty-three sediment tracer cores (Fig. 1b) placed in regions of different flow patterns (e.g. convergent, divergent, uniform) as predicted by the 2D model within different geomorphic units (e.g. riffle, bar, glide). Each tracer core contained individually sized grains taken from alluvial deposits along the Mokelumne River (~13,000 total), cleaned, measured, painted and sorted into four size classes: size class 1= 8-32 mm, size class 2= 32-64 mm, size class 3= 64-128 mm, and size class unsorted with d_{50} = 27 mm and d_{84} = 43 mm (Table 1). Existing substrates were excavated down 37 cm with a modified McNeal sampler and replaced with tracer rocks (Fig. 2). One core with each grain size class was placed in ~1 m intervals across a hydraulic region, yielding 6 different core-set locations (Fig. 1b). One of the 24 cores had flow over it that was too shallow to obtain data from for this study. Core points are denoted by location number and size class number (e.g. L1-sc1 for location 1 size class 1).

3.1 Observation Data

Field observations of depth and velocity were made at 0.6-m intervals across the two cross-sections on 11/21/02 three months after project construction when the discharge was 7.73 $m^3 s^{-1}$, while depth and vertical velocity profiles at the 23 tracer-core points were collected through January 2003 when discharge was at a low spawning/incubation flow rate of 7.51 $m^3 s^{-1}$.

Accepted

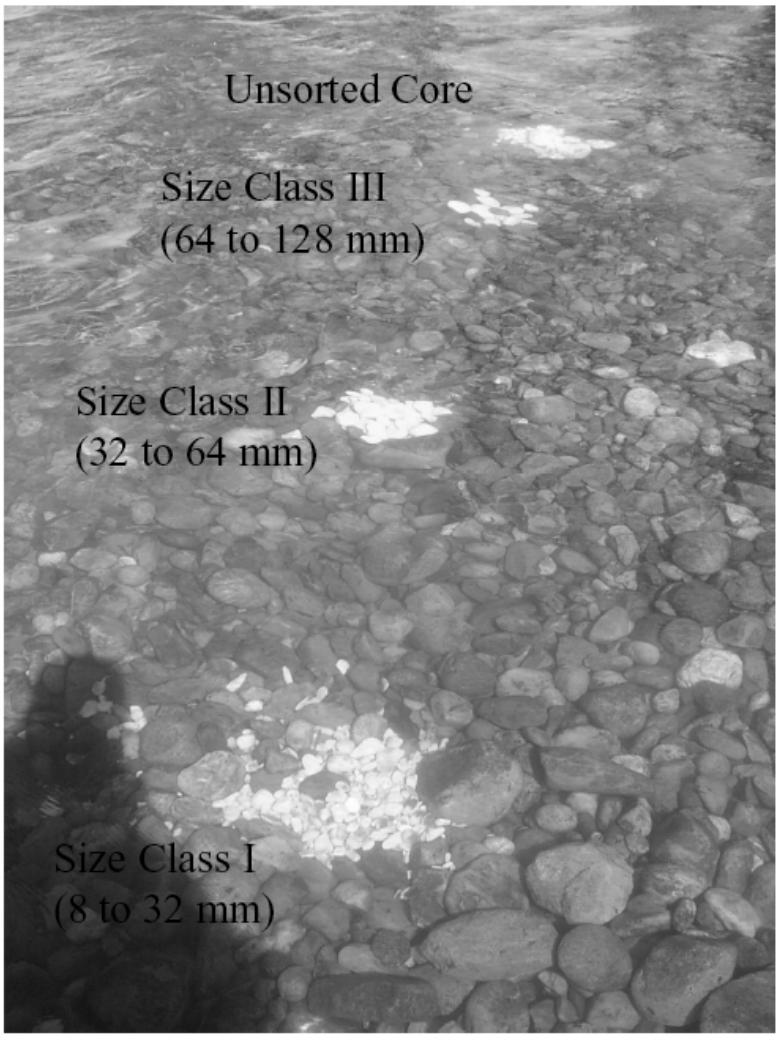
Unsorted Core
Size Class III
(64 to 128 mm)
Size Class II
(32 to 64 mm)
Size Class I
(8 to 32 mm)

Figure 2

For reference, the statistical bankfull discharge (Q1.5) prior to Camanche Dam construction was 120 m^3 s^{-1}. In all cases, depth was measured using a stadia rod to a resolution of ±1 cm and point velocity was measured using an electromagnetic Marsh-McBirney Flo-Mate (±33 mm s^{-1} root mean square) sampling at 30 Hz and averaged over 10 seconds. For cross-section velocity data, a depth-setting wading rod was used to position the sensor at 0.6 of the depth to obtain a measure of the depth-averaged velocity. For vertical velocity profiles over tracer cores, the diameter of the sensor head (3 cm) limited the resolution of the profile and constrained the number of points obtainable depending on water depth at each point. Thus, measurements were made at elevations of 2 and 5 cm above the bed, and then at 5-cm intervals through depth yielding 3-10 measurements per profile. The depth-averaged velocity at a tracer-core point (U) was calculated as the mean of vertical profile measurements.

3.2 2D Hydrodynamic Modelling

The two dimensional (depth-averaged) Finite Element Surface Water Modelling System model code (Froehlich, 1989) and Surface-water Modelling System (SMS) graphical interface (Environmental Modeling Systems, Incorporated) were used to predict site hydrodynamics at the 0.1-1 m scale relevant to microhabitat utilization and sediment entrainment. This 2D model uses a wetting and drying routine to determine channel boundary location. An element is "dry" when depth is below a user-defined threshold (set at 1 D_{90} ~0.12 m here) at all of its nodes. Model output included point-predictions of water depth, water velocity, and bed shear velocity. The equations built into the model for estimating bed shear velocity at each node were

$$u^* = U\sqrt{C_d} \quad \text{and} \quad C_d = 9.81\frac{n^2}{d^{1/3}} \tag{1,2}$$

where u* is shear velocity, U is depth-averaged velocity, C_d is the drag coefficient, n is

Accepted

Manning's n, and d is water depth (Froehlich, 1989). Shear velocity and Shields stress may be calculated from the available data, but this was not necessary for the assessment of uncertainty sought in this study, for which values of u* were appropriate.

Pasternack et al. (2004) and Wheaton et al. (2004 B) detail validation and utilization of the model on the Mokelumne River. A site DEM was made in AutoCAD Land Desktop 2002i based on 3,185 points surveyed with a Topcon GTS802A total station on a staggered-grid with supplemental features (average density of 0.88 pts m^{-2}). Point data augmentation (e.g. interpolation and user-specified spacing along contours) improved the DEM in areas with inadequate data. Refined topographic point and breakline data were exported to SMS. The 2D mesh was generated using a built-in adaptive tessellation algorithm without reference to the independently located depth and velocity measurement points. This independence provided a fair test of the accuracy of a 2D model without special attention to the mesh in the vicinity of validation locations. Node elevations were interpolated from imported DEM data using a TIN-based scheme. The mesh covered 16,930 m^2 of channel and banks with 23,957 computational nodes comprising 7830 elements, with the highest density near boulder clusters. The mesh's node density varied, but averaged 1.42 pts m^{-2}, which was significantly higher than that for the DEM.

Other than topography, the model's boundary conditions were steady state discharge (7.25 m^3 s^{-1}), corresponding water surface elevation at the downstream boundary (25.11 m in the NAVD88 vertical datum system), Manning's n bed roughness for well-mixed, placed gravels (0.043), and eddy viscosity (0.028 m^2 s^{-1}). Discharge was obtained from Camanche Dam (USGS station #11323500) for the flow used to compare pre-project, alternate design, and post-project conditions, so it was 5% lower than the average discharge of the field observations, which is a

Accepted

small unaccounted source of error. Water surface elevations associated with the studied flows were surveyed using the aforementioned total station with a vertical accuracy of ±2 cm. Manning's roughness (n) was estimated as 0.043 using a standard linear summation method (McCuen 1989; Pasternack et al., 1994) over the spatially explicit Strickler's equation for roughness because the bed was artificially created using a homogenized source of gravel. A constant eddy viscosity value for the model was estimated from pre-project, cross-section based, field observations of depth and velocity; as $\nu = C\, u^* R_h$ (Froehlich, 1989), where $C = 0.6$, R_h = hydraulic radius, and u^* was estimated using independent depth-averaged velocity data and the global z_0 velocity profile method explained below (using velocity at 0.6 of depth as depth-averaged velocity). Field estimated ν-values ranged from $9.3\ 10^{-4}$ to 0.033 $m^2\ s^{-1}$, with a mean of 0.015 $m^2\ s^{-1}$. The minimum stable value attainable with the model and subsequently used to obtain all results was 0.0279 $m^2\ s^{-1}$. Field estimates and the final model value were in the same range to those reported by Pasternack et al. (2004) and Wheaton et al., (2004 B).

Horizontal coordinates of cross-section endpins and tracer cores were located within 5 cm using a GTS802A total station and imported into the 2D modelling domain. For the cross-sectional evaluation, model predictions at computational nodes along the line between endpins were extracted and plotted on the same graph with the cross sectional field data, with no explicit matching of measurement locations. For tracer core comparisons, model depths and velocities at the exact locations of field measurement were obtained using TIN-based interpolation. Specifically, the centroid of an element is calculated, triangles are constructed in the element through the centroid, and then linear interpolation along the triangles is used to obtain data values. Since these data are from matching locations, predicted versus observed scatter plots and regression analysis were used to evaluate predictive accuracy.

Accepted

3.3 Velocity Profiles

The vertical velocity profile for steady, uniform, subcritical flow in a wide, straight channel with total roughness dominated by skin friction may be logarithmic over the whole flow depth (Wilcock, 1996). To assess this for tracer-core locations within the rehabilitation site with a known bed material size, whole vertical velocity profiles were inspected for their shape and fitted with the logarithmic function

$$\frac{u}{u*} = 5.75 log_{10}\left(\frac{30.2z}{k_s}\right) \quad (3)$$

where u is velocity in the direction of flow, z is elevation above the bed and $k_s = 33z_o$ is the boundary roughness (Smart, 1999). The bed material placed at the site was the same across the whole area, so that reduced the error that would otherwise result from having a variable k_s. For each tracer core, the bed material was nearly uniform in grain size, further reducing potential error in estimating k_s. When the stated assumptions are violated, eq. (3) only applies to the bottom ~20% of the water column, above a near-bed "roughness" region and below an outer "turbulent" region (Wiberg and Smith, 1991; Wilcock, 1996). To test this assumption, depth-normalized velocity profiles may be assessed for slope breaks differentiating log-linear inner and outer profiles (Lawless and Robert, 2001), yielding skin friction and form drag, respectively. Unfortunately, in this study the size of the sensor head and low water depth limited the number of points available for profiles and proximity to the bed introducing uncertainty (Biron et al., 1998). However, previous studies have used a similar approach and successfully resolved profiles (e.g. Robert, 1997). Tiny sensors (<5 mm) may be more precise, but their measurements are strongly influenced by strong velocity variability induced by complex scales of bed

Accepted

roughness (Lawless and Robert, 2001), which is beyond the scope of eq (3) to address anyway.

3.4 Shear Velocity Estimation

Shear velocity in the form of u* was estimated from field measurements using five methods and from model output using three methods, because there is no general consensus as to which approach is best for shallow gravel-bed river conditions. Eqs. (1,2) were applied to tracer-core and model-output datasets using depth-averaged velocity and were additionally applied to the field data substituting the near-bed (z = 2 cm) velocity for the depth-averaged velocity. Whole velocity profiles were fitted with eq. (3) and values of u* and k_s were obtained as a third method of estimating u* from the field data. Wilcock (1996) compared the utility of depth-averaged velocities, point velocities in the lowest 20% of the flow, and slopes of whole velocity profiles for estimating local bed shear velocity. He noted that errors in u* estimates from the slope of a velocity profile are ~8-9 times larger than those in u* estimates based on depth-averaged velocities. Thus, u* was calculated two different ways using the depth-integrated form of (3) assuming that $d >> z_0$ (Wilcock, 1996; Smart, 1999)

$$u^* = \frac{U}{5.75 log_{10}\left(12.2\frac{d}{33 z_o}\right)} \quad (4)$$

where z_0 was calculated once as a global constant for all locations equal to $D_{84}/10$ (Wilcock, 1996) using the overall pebble-count grain size distribution for the site to get D_{84} and once individually derived for each location from the log-velocity profile according to eq. (3). The two measures of u* from eq. (4) were used for both tracer-core and model-output datasets.

To account for the error in u* estimates due to limitations in field measurement, Wilcock's (1996) linear error propagation formula was utilised for the depth-averaged u* estimates. Expressed in proportional form, the standard error, $\alpha(u_*)$, for u_* was estimated as

Accepted

$$\frac{\alpha(u^*)}{u^*} = \sqrt{\left(\frac{\alpha_U}{U}\right)^2 + \left(\frac{\alpha_d}{d\xi_d}\right)^2 + \left(\frac{\alpha_{D_p}}{D_p\xi_d}\right)^2} \quad (5)$$

where α_U and α_d are errors in U and d respectively, α_{Dp} is taken to be $D_{90}/16$, D_p is taken as D_{84}, and $\alpha_d = \ln[11d/(3D_{84})]$ (Wilcock, 1996). The error in depth measurement was 1 cm. Because the method for u* estimation assumes a logarithmic velocity profile, the error metric used as an estimate of α_U was taken as the deviation of actual profiles from the logarithmic ideal, which also accounts for sensor error. This was calculated as the mean plus two standard deviations in the data set (n=23) of absolute values of the difference between the calculated mean velocity for a profile and the velocity value at 0.6*depth taken from the fitted logarithmic curve.

4. RESULTS

4.1 Velocity Profiles

All twenty-three vertical velocity profiles had statistically significant, highly correlative fits with a logarithmic profile over the whole flow depth (Fig. 3). Locations L2_sc2 and LS-scU had S-shaped profiles, while L2_sc1 had a nearly uniform profile for the upper 80% of depth overlying a linear profile for the lower 20% of depth. Individual log-profiles were significantly different in velocity magnitudes and velocity gradient as a function of depth. The deepest areas- L2 and L4- had more points in their velocity profiles allowing better resolution of the flow regions. Underlying tracer-core grain-size distributions did not explain differences between sites. The average ratio of velocity at 0.6*depth to depth-average velocity was 1.06 (±0.14 SD). The ratio of velocity at 2 cm above the bed to depth-averaged velocity showed more variability, averaging 0.41 (±0.23 SD). Locations L1_sc3 and L2_sc1 had upstream-directed near-bed

Accepted

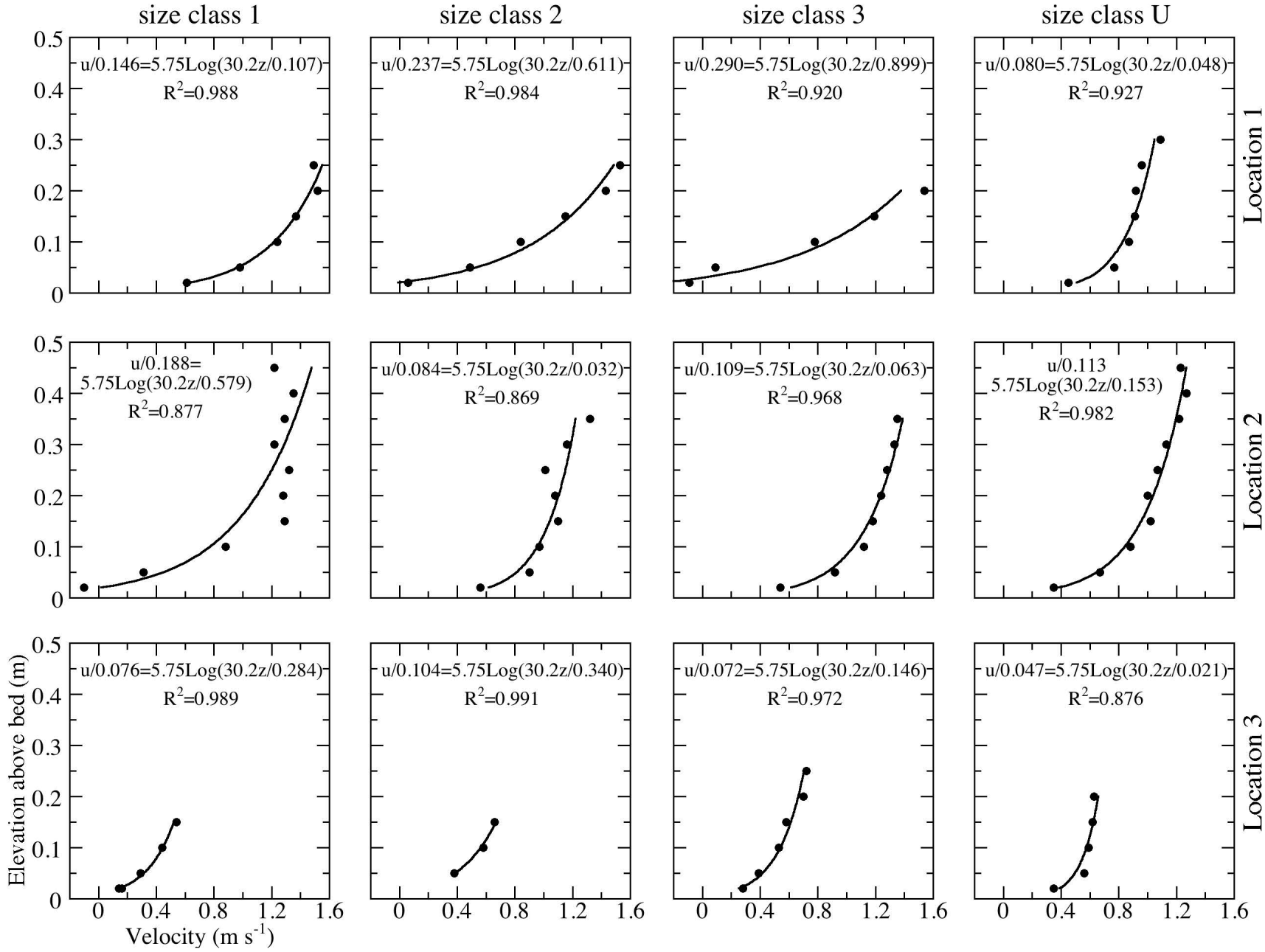
size class 1
size class 2
size class 3
size class U
u/0.146=5.75Log(30.2z/0.107)
R2=0.988
u/0.237=5.75Log(30.2z/0.611)
R2=0.984
u/0.290=5.75Log(30.2z/0.899)
R2=0.920
u/0.080=5.75Log(30.2z/0.048)
R2=0.927
Location 1
u/0.188=
5.75Log(30.2z/0.579)
R2=0.877
u/0.084=5.75Log(30.2z/0.032)
R2=0.869
u/0.109=5.75Log(30.2z/0.063)
R2=0.968
u/0.113
5.75Log(30.2z/0.153)
R2=0.982
Location 2
u/0.076=5.75Log(30.2z/0.284)
R2=0.989
u/0.104=5.75Log(30.2z/0.340)
R2=0.991
u/0.072=5.75Log(30.2z/0.146)
R2=0.972
u/0.047=5.75Log(30.2z/0.021)
R2=0.876
Location 3
Elevation above bed (m)
Velocity (m s-1)
0
0.1
0.2
0.3
0.4
0.5
0.4
0.8
1.2
1.6

Figure 3a

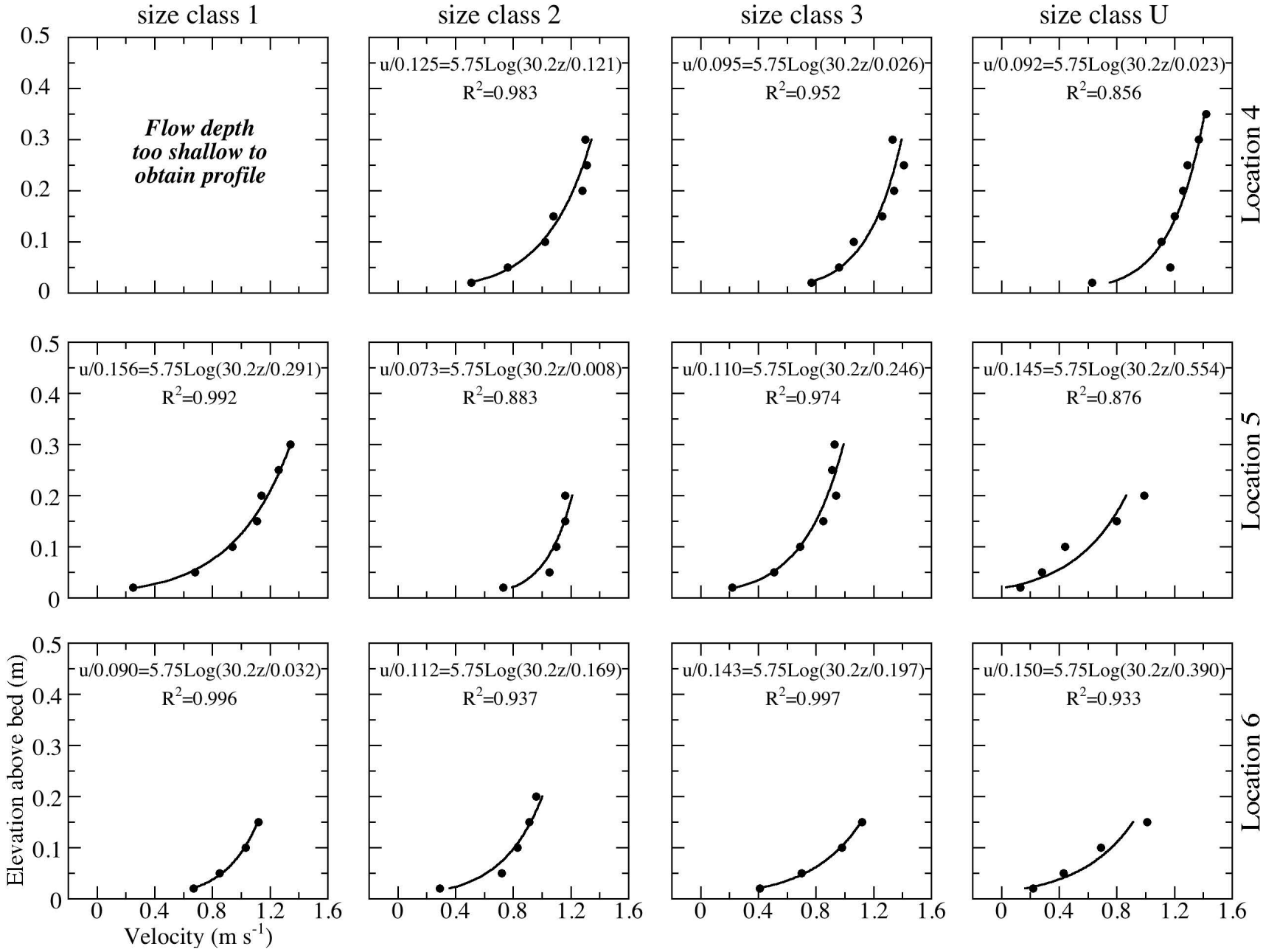
size class 1
size class 2
size class 3
size class U
Location 4
Location 5
Location 6
Flow depth too shallow to obtain profile
u/0.125=5.75Log(30.2z/0.121)
R2=0.983
u/0.095=5.75Log(30.2z/0.026)
R2=0.952
u/0.092=5.75Log(30.2z/0.023)
R2=0.856
u/0.156=5.75Log(30.2z/0.291)
R2=0.992
u/0.073=5.75Log(30.2z/0.008)
R2=0.883
u/0.110=5.75Log(30.2z/0.246)
R2=0.974
u/0.145=5.75Log(30.2z/0.554)
R2=0.876
u/0.090=5.75Log(30.2z/0.032)
R2=0.996
u/0.112=5.75Log(30.2z/0.169)
R2=0.937
u/0.143=5.75Log(30.2z/0.197)
R2=0.997
u/0.150=5.75Log(30.2z/0.390)
R2=0.933
Elevation above bed (m)
Velocity (m s-1)
0
0.1
0.2
0.3
0.4
0.5
0.8
1.2
1.6

Figure 3b

velocities due to flow separation downstream of grain protrusions.

4.2 2D Model Results

The model region contained three riffles and two pools, with the largest riffle being artificially constructed and including significant heterogeneity. According to the design and post-project model predictions (Fig. 4), initially planar flow over the upstream riffle crest was split into a main streamtube and a secondary streamtube by a boulder complex, where a streamtube is a 2D flow region of approximately parallel flow trajectories. Downstream the main streamtube was split again by a second boulder complex, with the majority of it constricted into a peripheral pool. Flow from secondary streamtube moved slower and diverged strongly around the second boulder complex and over the shallower riffle zone to cover the majority of channel width. The main flow tube was highly constricted along the left bank, but continued through a sequence of mid-depth diverging glides and constricting pools with high velocity variability. Meanwhile, the secondary streamtube was divided by a central longitudinal bar yielding more local divergence and convergence zones providing significant velocity variability. The shallow glide along the right bank was slow moving. At the end of the central bar, the main stream tube diverged out of a peripheral pool across a riffle crest and converged with the secondary streamtubes to yield high velocities over a stream-wide glide. An exposed sand and mud bar constricts the cannel at this point accelerating the flow into the first of two deep pools in the study area. After that, flow strongly diverges over a wide, flat riffle and then becomes planar until it converges strongly yielding very high velocities over the second major pool. Finally, flow diverges over the last riffle entrance and flows planar over the riffle crest.

Accepted

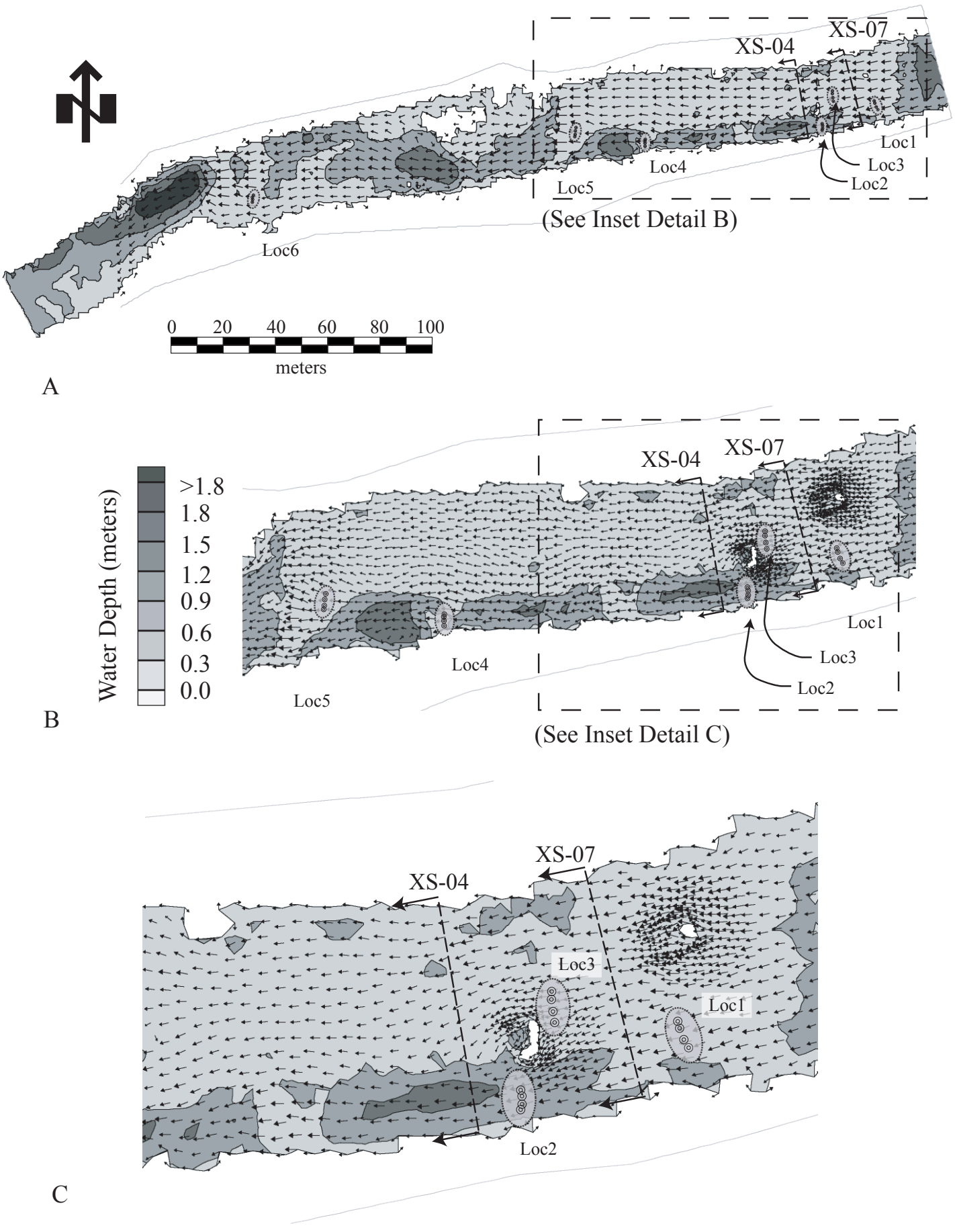
XS-04
XS-07
Loc1
Loc2
Loc3
Loc4
Loc5
Loc6
(See Inset Detail B)
0 20 40 60 80 100
meters
A
Water Depth (meters)
>1.8
1.8
1.5
1.2
0.9
0.6
0.3
0.0
B
(See Inset Detail C)
C

Figure 4

4.3 Depth Prediction

Model depth predictions were compared against cross-sectional data for spatial patterns and tracer-point data for quantitative analysis. For the cross-sections, the DEM and 2D model captured the cross-channel variability of bed features with a relief >20 cm but over-predicted depth (Fig. 5a,c). At tracer-core locations model predictions deviated from observed depths by an average of 21 % (±17 % SD), with a tendency to over-predict (Table 1; Fig. 6). No trend in predictability was found as a function of depth or local bed material grain size, on the chance that local bed roughness could be a systematic source of error. The L2 points located on a pool entrance slope along the left bank (Fig. 1b) had the worst predictability. Of those, the one closest to the bank had the most under-predicted depth (45 %) of all measured locations. In the 2D model this point was located between wet and dry nodes that were only 1 m apart. Model predictions in this zone should be treated with scepticism, because no effort was made address sub-grid scale variations in bank topography. If the bed elevation of the measurement point is manually subtracted from the water surface elevation of the adjacent wet node, then the resulting depth is predicted to be 0.41 m, which is within 18 % of the measured value. The point with the worst over-prediction (71 %) was L1_sc3 located on the first riffle crest. Since this location had the coarsest bed material (D_{90} =153 mm), it is possible that the wading rod was randomly placed on top of a protruding cobble. Such an effect is at the sub-grid scale of the model.

4.4 Velocity Prediction

Similar to the depth results, cross-sectional variations revealed the spatial pattern of velocity prediction accuracy while tracer-core comparisons provided quantitative metrics of accuracy. Due to short sampling times and the location of some sites in the vortex shedding zone

Accepted

Table 1. Field-measured and model-predicted bed and flow characteristics at tracer core locations.

	Grain size parameters			Measured		Model-predicted	
Site	D_{50} (m)	D_{84} (m)	D_{90} (m)	d (m)	U (ms^{-1})	d (m)	U (ms^{-1})
Yellow tracers at top flat riffle							
L1-scU	0.027	0.043	0.055	0.33	0.85	0.41	0.80
L1-sc1	0.021	0.028	0.029	0.32	1.20	0.36	0.96
L1-sc2	0.046	0.058	0.060	0.33	0.92	0.33	0.93
L1-sc3	0.088	0.138	0.153	0.24	0.70	0.41	0.89
Green tracers at front end of pool along left bank							
L2-scU	0.027	0.043	0.055	0.50	0.98	0.62	0.82
L2-sc1	0.021	0.028	0.029	0.50	1.01	0.27	0.16
L2-sc2	0.046	0.058	0.060	0.40	1.01	0.55	0.33
L2-sc3	0.088	0.138	0.153	0.40	1.12	0.55	0.58
Orange tracers on shallow bar in center of channel							
L3-scU	0.027	0.043	0.055	0.26	0.55	0.25	0.63
L3-sc1	0.021	0.028	0.029	0.18	0.36	0.24	0.51
L3-sc2	0.046	0.058	0.060	0.18	0.44	0.21	0.49
L3-sc3	0.088	0.138	0.153	0.28	0.53	0.31	0.57
Blue tracers between pools							
L4-scU	0.027	0.043	0.055	0.40	1.18	0.46	1.06
L4-sc2	0.046	0.058	0.060	0.36	1.04	0.40	1.09
L4-sc3	0.088	0.138	0.153	0.36	1.16	0.45	1.17
Pink tracers along pool to riffle transition							
L5-scU	0.027	0.043	0.055	0.26	0.53	0.19	0.88
L5-sc1	0.021	0.028	0.029	0.32	0.96	0.26	0.88
L5-sc2	0.046	0.058	0.060	0.24	1.04	0.24	0.84
L5-sc3	0.088	0.138	0.153	0.34	0.72	0.26	0.89
Dark green/white tracers on unchanged riffle downstream of project							
L6-scU	0.027	0.043	0.055	0.18	0.59	0.18	1.05
L6-sc1	0.021	0.028	0.029	0.20	0.92	0.19	0.93
L6-sc2	0.046	0.058	0.060	0.22	0.74	0.16	1.11
L6-sc3	0.088	0.138	0.153	0.20	0.80	0.16	1.19

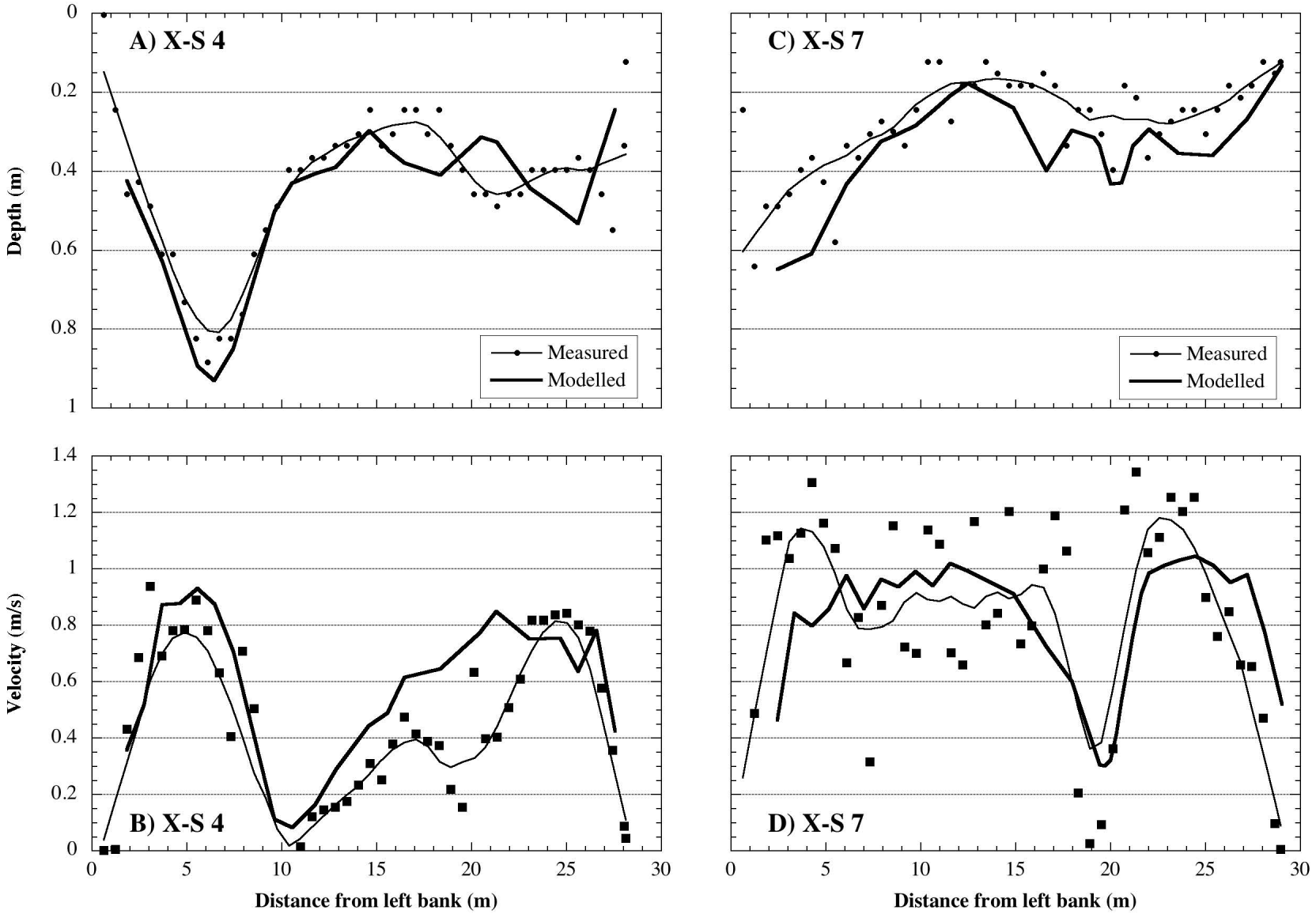
A) X-S 4
C) X-S 7
B) X-S 4
D) X-S 7
Measured
Modelled
Depth (m)
Velocity (m/s)
Distance from left bank (m)
Distance from left bank (m)

Figure 5

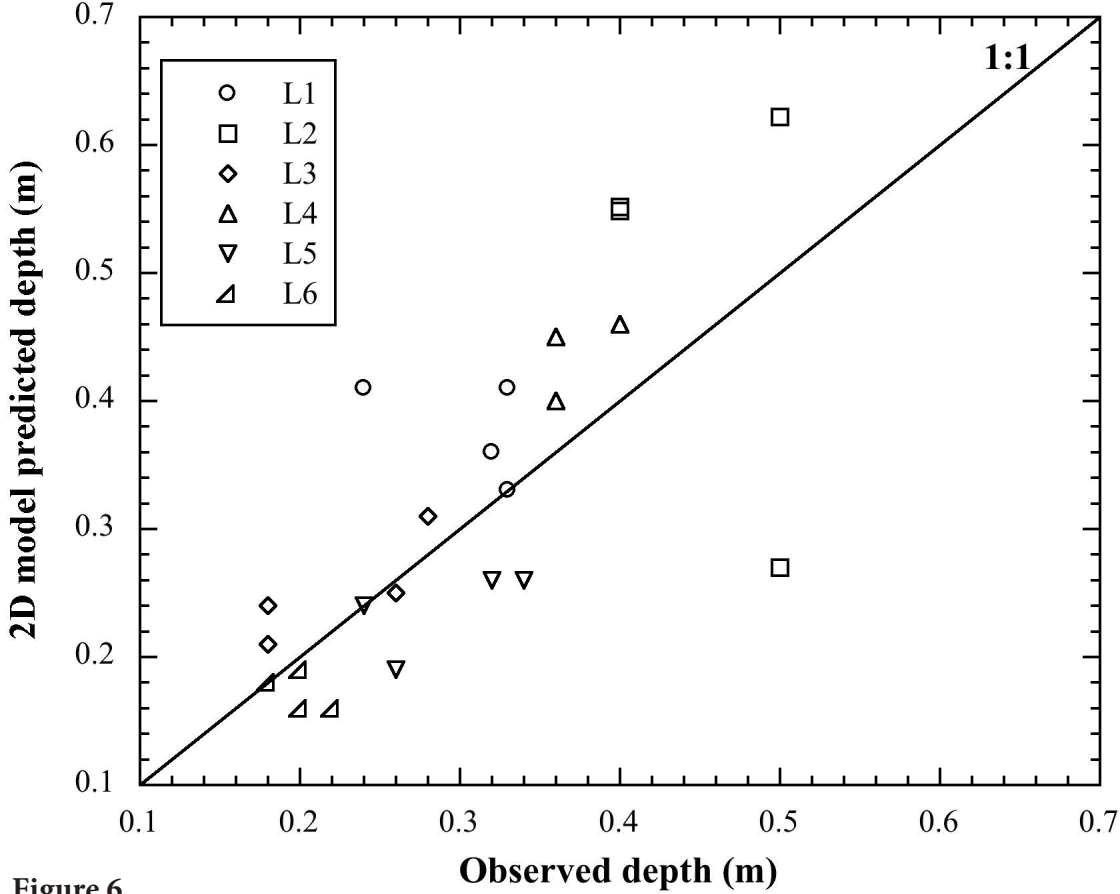
0.7
0.6
0.5
0.4
0.3
0.2
0.1
2D model predicted depth (m)
L1
L2
L3
L4
L5
L6
1:1
0.1
0.2
0.3
0.4
0.5
0.6
0.7
Observed depth (m)

Figure 6

downstream of placed boulders, measured velocities showed high fluctuations over short lateral distances. To counter this effect, a curve was fit to the data using the locally weighted Least Squared error method. Both cross-sections had structured lateral variations in velocity magnitude of 0.1-1 m s^{-1} at the 1-10 m spatial scale due to converging/diverging and accelerating/decelerating streamtubes around and over constructed bar features. Observed lateral variations in velocity were captured by the 2D model (Fig. 4b,d). Cross-section 4 showed a general overprediction, with a 30-50% overprediction over the central bar top. Given that both depth and velocity were overpredicted, optimization of the bed roughness parameter could not improve predictions of one without making the other worse. Cross-section 7 showed a close match between observed and predicted velocities. At tracer-core locations, velocities predicted by the 2D model deviated from velocity-profile mean velocities by an average of 29 % (±26 % SD) (Table 1; Fig. 7a).

Errors in velocity prediction were not a function of depth, local bed-material grain size, or velocity. Instead, the absolute value of error in depth prediction accounted for 56% of the variability in the absolute value of velocity error, with $p<0.0001$ (Fig. 7b). According to the trend (excluding 2 outliers), each additional 1% increase in depth prediction error yielded a 1.5% error in velocity prediction overall. The data shows that where depth prediction error was 0-20 %, velocity prediction error randomly varied between 0-20 % also, whereas sites with depth prediction error >25 % had velocity prediction errors varying randomly between 40-85%. The locations with the best predictability occurred on riffle tops (L1, L3, and L5). Those with the worst predictability occurred at the pool entrance close to the river-left bank (L2) and at the most downstream riffle (L6). Depths at L2 points were over-predicted, causing an under-prediction in velocity, and this effect was compounded by the retarding effect of the nearby bank in the model.

Accepted

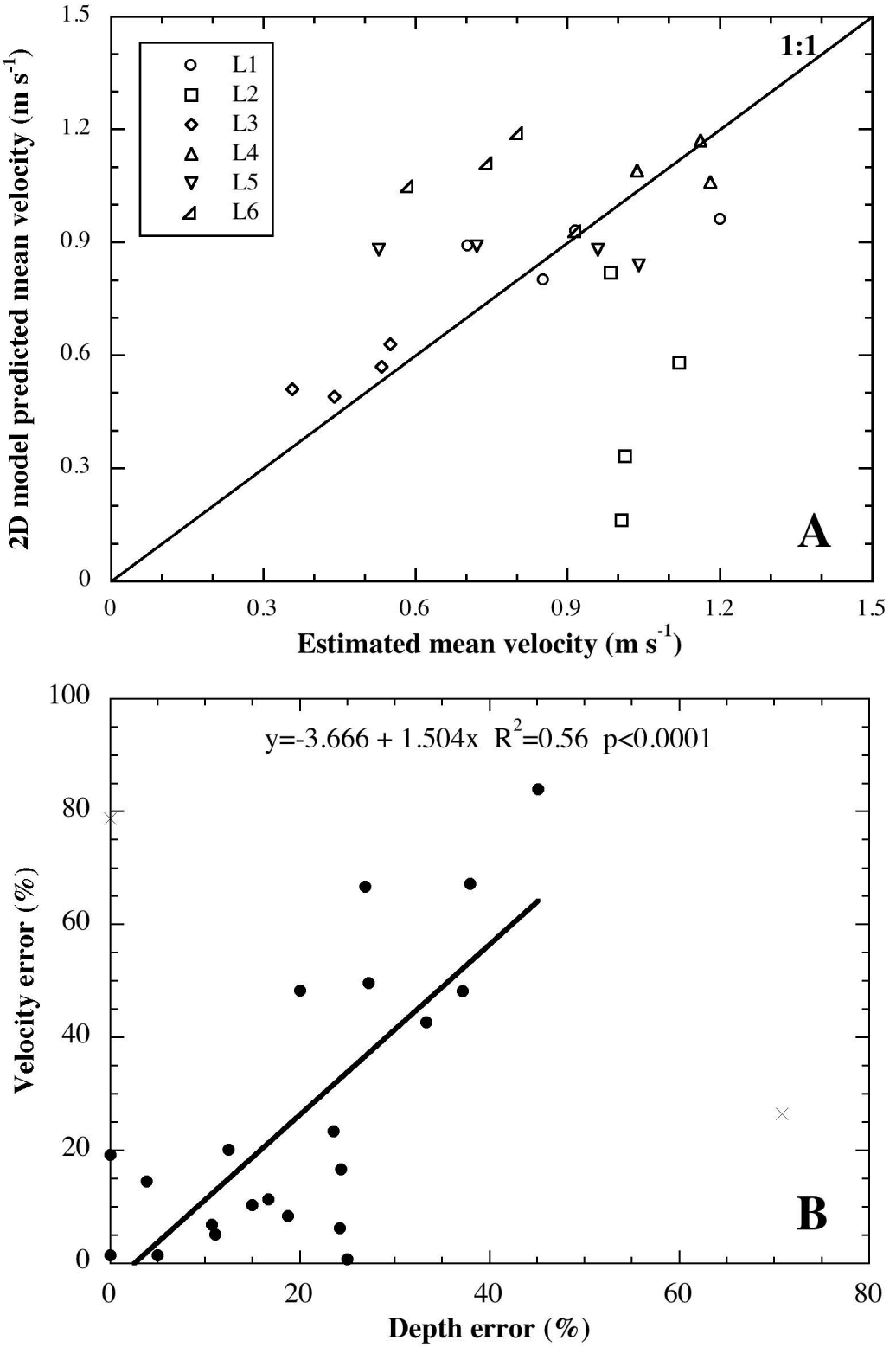
1.5
1.2
0.9
0.6
0.3
0
0
0.3
0.6
0.9
1.2
1.5
2D model predicted mean velocity (m s-1)
Estimated mean velocity (m s-1)
L1
L2
L3
L4
L5
L6
1:1
A
100
80
60
40
20
0
0
20
40
60
80
y=-3.666 + 1.504x R2=0.56 p<0.0001
Velocity error (%)
Depth error (%)
B

Figure 7

For the highly over-predicted velocities of the L6 tracer points, the model had under-predicted the depth over sorted cores yielding the shallowest predicted depths of all test points. This depth-error produced skimming flow close to the Fr supercritical threshold, which may have increased the error. For L6-scU, there was no error in depth prediction, but the velocity was overpredicted by 78 %. The velocity profile for this spot showed very low velocities (Fig. 3) that may have been so low because of the local roughness due to the unsorted bed material, which was not represented in the 2D model.

4.5 Total Shear Velocity Prediction

Differences among field-observational methods for estimating u* were larger than those between corresponding field estimation and model-prediction u* methods (Table 2). Minimum and maximum estimates of total shear velocity based on four observational methods over each tracer core differed by an average of 64 % with a range of 5.6-160 %. A comparison of field-estimation methods for u* using U in eq. (1,2) versus using it in eq (4) shows that there is only a small difference between the two (Fig. 8). Meanwhile, shear velocities predicted by the 2D model deviated from field-estimated values by lower averages (and ranges) of 36 % (0.6-99 %), 31 % (0.6-92 % range), 31 % (0.4-103 %) using comparable eqs. (1,2), eq. (4) with a global z_o, and eq. (4) with a local z_o, respectively. For this case, this result contradicts the qualitative remarks of Lane et al. (1999) who state that their 2D model over-predictions of bed shear stress were “ridiculous”. For the method of eqs. (1,2), field-estimated and model predicted values of C_d were similarly low (~0.02-0.03), with the only source of difference stemming from differences in depth, according to eq. (2). For the method of eq. (4) with a global z_o, more than half of predicted values fell within the 95% confidence limits of field-estimation uncertainty

Accepted

Table 2. Field-estimated and model-predicted parameters and shear velocities at tracer core locations.

Site	Field estimated ks	Field estimated Cd	Field-estimated u* (ms^{-1})* a	b	c	d	e	Model-predicted Cd	Model-predicted u* (ms^{-1})* a	d	e
Yellow tracers at top flat riffle											
L1-scU	0.048	0.026	0.138	0.073	0.080	0.130	0.077	0.024	0.125	0.113	0.069
L1-sc1	0.107	0.027	0.196	0.099	0.146	0.186	0.134	0.025	0.153	0.142	0.103
L1-sc2	0.611	0.026	0.149	0.010	0.237	0.141	0.195	0.026	0.151	0.142	0.198
L1-sc3	0.899	0.029	0.120	0.015	0.290	0.122	0.239	0.024	0.139	0.126	0.208
Green tracers at front end of pool along left bank											
L2-scU	0.153	0.023	0.149	0.053	0.113	0.129	0.107	0.021	0.120	0.101	0.084
L2-sc1	0.579	0.023	0.152	0.015	0.188	0.133	0.171	0.028	0.027	0.027	0.037
L2-sc2	0.032	0.025	0.159	0.088	0.084	0.144	0.081	0.022	0.049	0.042	0.025
L2-sc3	0.063	0.025	0.176	0.085	0.109	0.160	0.103	0.022	0.086	0.074	0.050
Orange tracers on shallow bar in center of channel											
L3-scU	0.021	0.028	0.093	0.059	0.047	0.093	0.044	0.029	0.107	0.108	0.051
L3-sc1	0.284	0.032	0.064	0.029	0.076	0.072	0.070	0.029	0.087	0.089	0.088
L3-sc2	0.34	0.032	0.079	0.025	0.104	0.088	0.094	0.031	0.086	0.091	0.097
L3-sc3	0.146	0.028	0.089	0.047	0.072	0.086	0.068	0.027	0.093	0.089	0.070
Blue tracers between pools											
L4-scU	0.023	0.025	0.185	0.099	0.092	0.168	0.088	0.023	0.162	0.144	0.077
L4-sc2	0.121	0.025	0.166	0.081	0.125	0.148	0.116	0.025	0.171	0.155	0.118
L4-sc3	0.026	0.025	0.185	0.123	0.095	0.165	0.091	0.024	0.180	0.160	0.088
Pink tracers along pool to riffle transition											
L5-scU	0.554	0.028	0.089	0.022	0.145	0.089	0.121	0.032	0.156	0.171	0.246
L5-sc1	0.291	0.027	0.156	0.041	0.156	0.149	0.148	0.028	0.148	0.148	0.148
L5-sc2	0.008	0.029	0.178	0.125	0.073	0.181	0.071	0.029	0.144	0.146	0.057
L5-sc3	0.246	0.026	0.116	0.035	0.110	0.109	0.102	0.028	0.150	0.150	0.139
Dark green and white tracers on un-changed pre-existing riffle downstream of project											
L6-scU	0.39	0.032	0.105	0.039	0.150	0.117	0.136	0.032	0.188	0.209	0.243
L6-sc1	0.032	0.031	0.162	0.118	0.090	0.174	0.085	0.032	0.165	0.180	0.087
L6-sc2	0.169	0.030	0.129	0.050	0.112	0.134	0.107	0.033	0.203	0.235	0.182
L6-sc3	0.197	0.031	0.141	0.072	0.143	0.151	0.128	0.033	0.218	0.252	0.208

*Methods are a= eq(1,2) using U, b=eq(1,2) using u_bed, c=eq(3), d=eq(4) using global z_o, e=eq(4) using local z_o

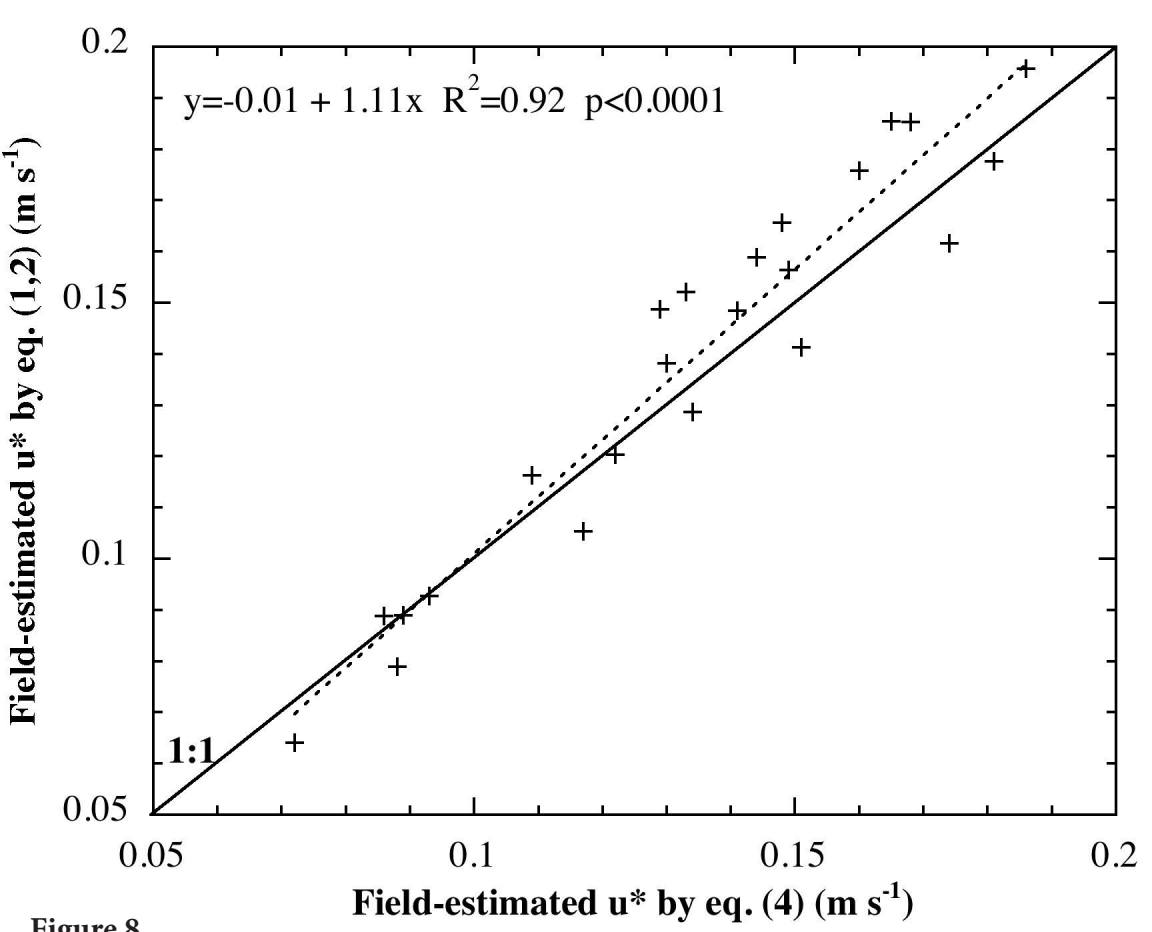
y=-0.01 + 1.11x R2=0.92 p<0.0001
1:1
Field-estimated u* by eq. (1,2) (m s-1)
Field-estimated u* by eq. (4) (m s-1)
0.05
0.1
0.15
0.2

Figure 8

predicted using eq. (5) (Fig. 9). 63 % of predictions using that method had less than 25% error. Of the 7 points with > 50% error, 3 were at L6 where depth was < 0.2 m (Fig. 3b) and 3 were at L2, whose challenging local conditions have already been described. The most poorly predicted point with an error of 91% was L5-scU. Error in the absolute value of velocity prediction accounted for 90% of the error in the absolute value of shear velocity model prediction (Fig. 10). When the 7 most poorly predicted points were corrected for velocity error, they had an average remaining error of 11 % (±7.3 % SD).

4.6 Bed Shear Velocity Prediction

Because of the lack of distinguishable inner and outer regions with distinct log-linear vertical velocity profiles (Fig. 3), the only available method for estimating bed shears stress using the field data was to use eq. (1,2) with u measured at the position closest to the bed over each tracer core. Compared to that estimated using eq. (1,2) with U, u* estimated using the near-bed velocity averaged 57 % lower, ranging from 27-93 % lower. The variability in the difference between total versus near-bed u* is primarily explained by the differing profile shapes (Fig. 3), with steeper velocity gradients as a function of depth corresponding to higher deviations between total and bed shear velocity (Fig. 11). Unfortunately, none of depth, depth-averaged velocity, or bed material grain size explain the variability in whole-profile vertical velocity gradient. Instead, that variability is due to a complex array of variability in bed topography and resulting 3D flow structure processes. In general steeper vertical velocity gradients occurred over flat riffles with planar 2D flow patterns (L1 and L6) whereas gentle gradients occurred over pools with convergent flow (L2), riffle exits with divergent flow (L3), and mid-depth glides (L4). An exception to this was tracer core L2-sc1, which had a sharp near-bed gradient underlying nearly

Accepted

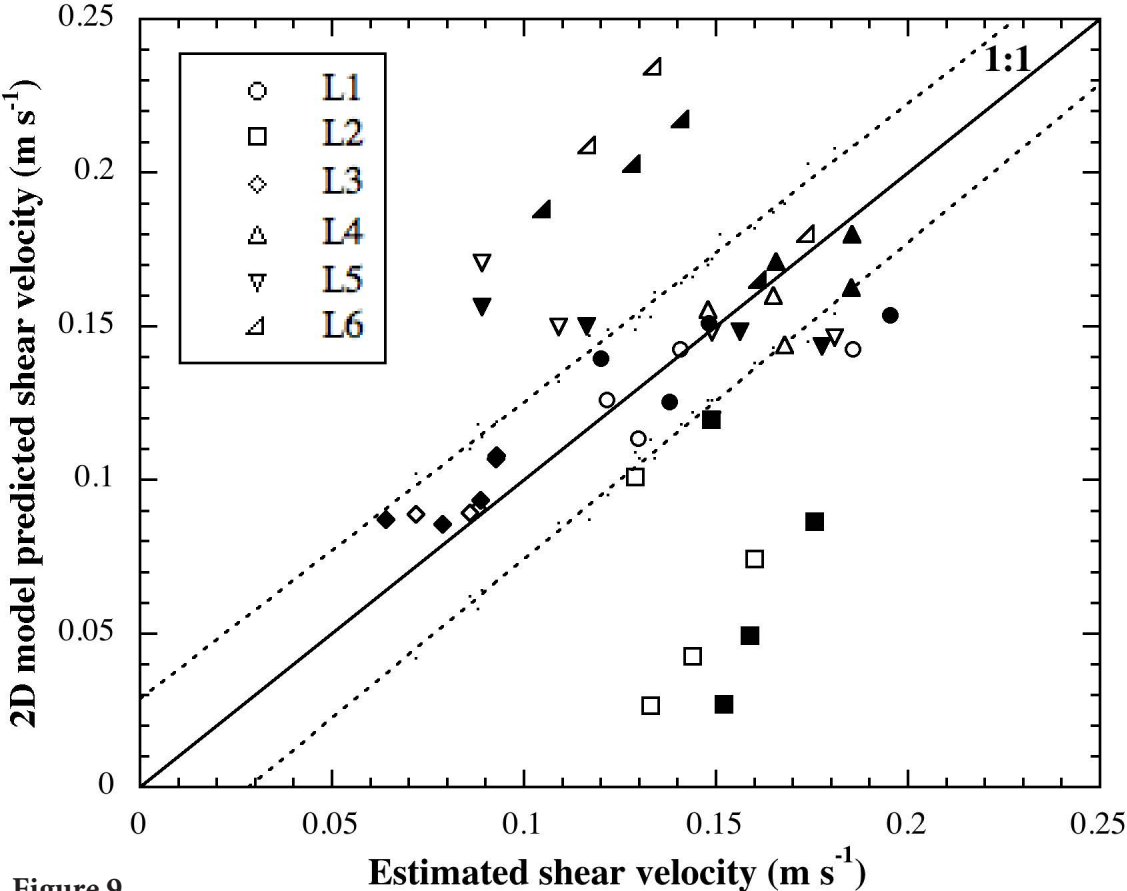
L1
L2
L3
L4
L5
L6
1:1
2D model predicted shear velocity (m s-1)
Estimated shear velocity (m s-1)
0
0.05
0.1
0.15
0.2
0.25

Figure 9

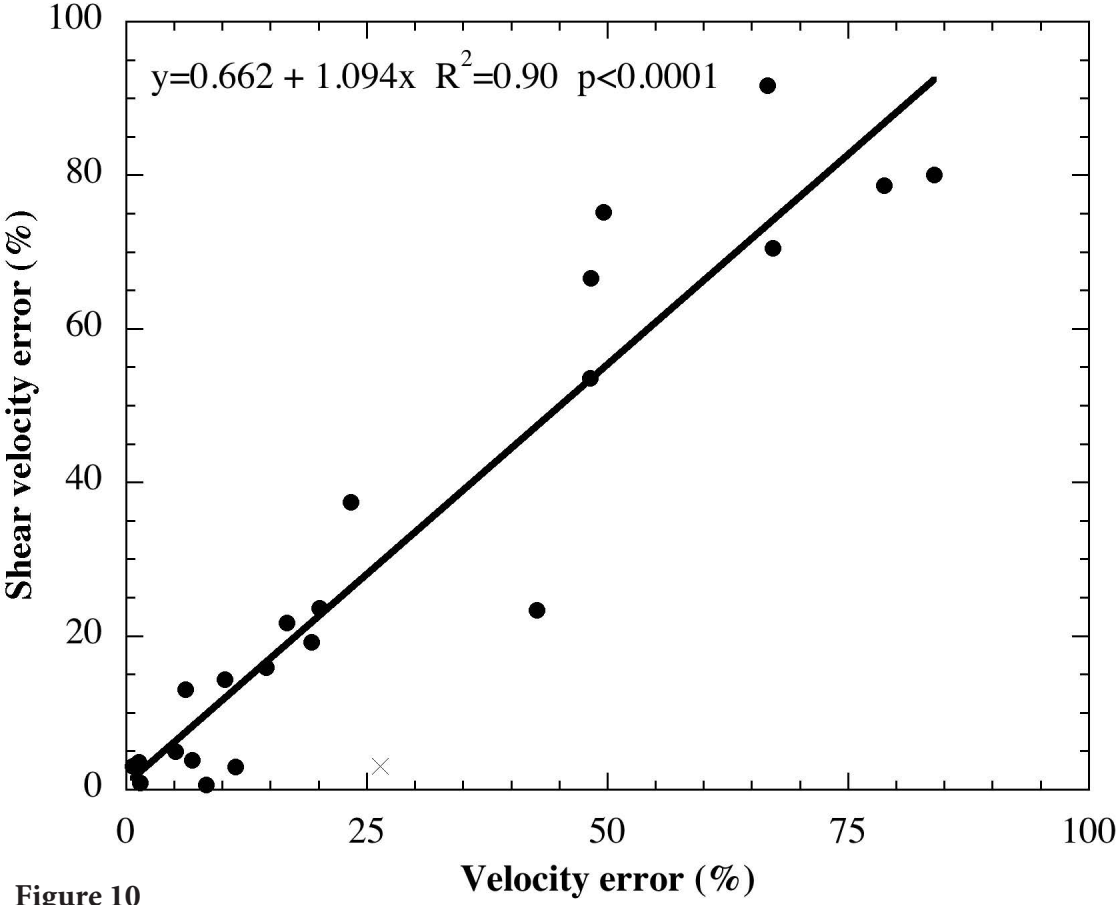
y=0.662 + 1.094x R²=0.90 p<0.0001
Shear velocity error (%)
Velocity error (%)
0
20
40
60
80
100
0
25
50
75
100

Figure 10

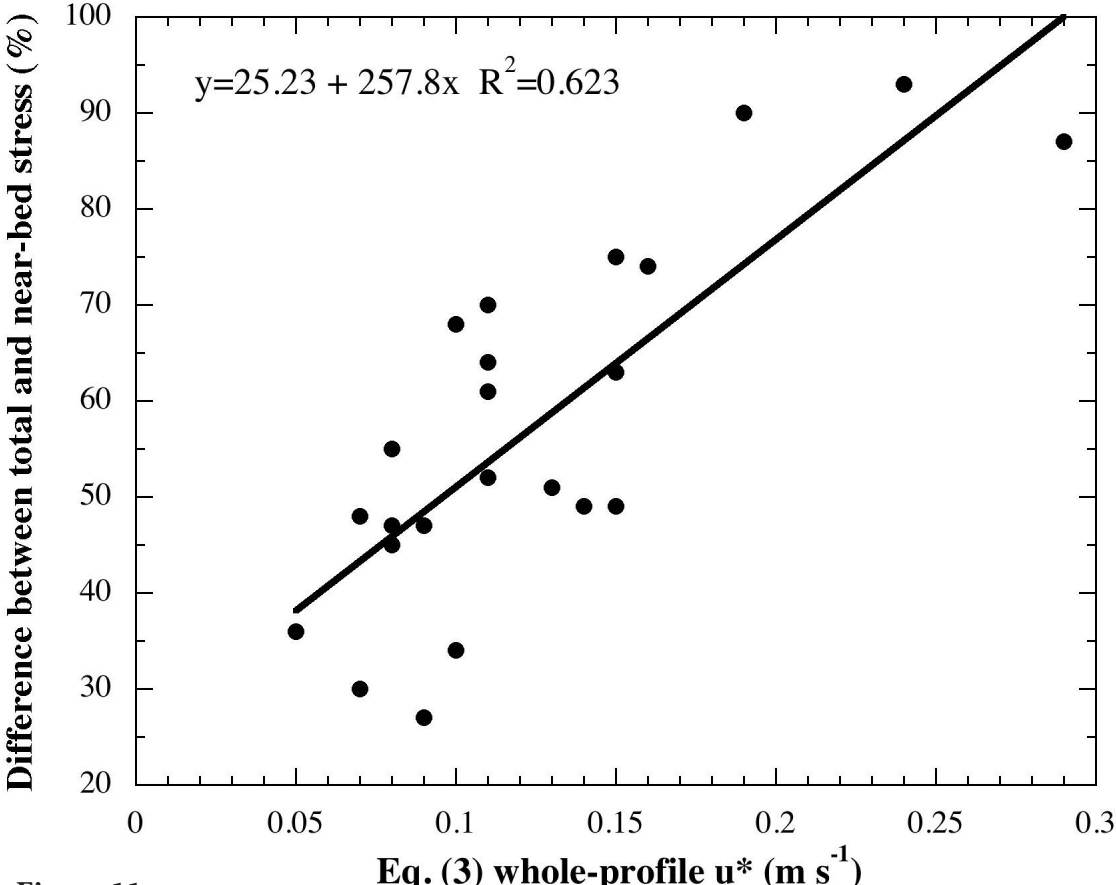
y=25.23 + 257.8x R^2=0.623
Difference between total and near-bed stress (%)
Eq. (3) whole-profile u* (m s^{-1})
100
90
80
70
60
50
40
30
20
0
0.05
0.1
0.15
0.2
0.25
0.3

Figure 11

uniform flow.

For practical application of 2D models for sediment entrainment prediction in shallow gravel-bedded rivers, an accurate estimate of near-bed u*, not total u* is needed. Despite the unaccountable sources of error inherent in the observed data due to the complex bed topography, a significant improvement in the prediction of near bed u* can be obtain by adjusting model output u* with a constant multiplier. Using the Solver add-on to Microsoft Excel, the constant reduction multiplier in total u*that yielded the lowest average absolute difference (29.5%) in total versus near-bed u*was evaluated and found to be 0.51, though the standard deviation went up from 0.19 to 0.29. This shift brings the 2D model prediction of u* well within the range of uncertainty for field estimation of near-bed u*. More studies are needed to determine the generality of a ~50% reduction in 2D model estimates to match observations, but the finding of this study substantiates that 2D models can be used to accurately estimate shear velocity in environmental management applications as long as significant effort is placed on accurately discretizing the topographic boundary condition and the difference between total and near bed shear stress estimates is accounted for.

5. DISCUSSION

In this study it was found that the error in 2D model predictions of depth, velocity, and shear velocity over well-mixed, double washed gravel averaged 21%, 29%, and 31%, respectively. These accuracies reflect the very challenging field conditions on a carefully constructed geomorphic-unit with highly complex 3D features by design. Depth error prediction was directly attributable to error in the DEM and thus was not primarily an error of the 2D model itself. More than half the error in velocity was in turn caused by depth error, and then 90% of the

Accepted

shear velocity error was caused by velocity error. Thus, the single most important factor in determining 2D model prediction accuracy is DEM accuracy.

Pasternack et al. (2004) addressed the topic of DEM accuracy in terms of the topographic survey (resolution and accuracy) and DEM generation methodology. In this study, the bed was surveyed with a resolution of 1 point every 1.14 m^2, which is quite high relative to previously published efforts and above that specified to capture typical gravel-bed morphology (Brasington et al., 2000). Even this resolution is still inadequate for comparison against typical 0.01-m scale positional measurements. Unlike sand-beds, gravel beds can have significant interlocking grain friction that is capable of sustaining complex pebble cluster morphologies, depressions, and bars at length scales of 0.001-1 m. These features may be created by flow processes and fish pedoturbation. It is now apparent that reducing the error of 2D model predictions at individual nodes from the 20-30% range to the <10% range must require higher survey-point densities than 1 point every 1.2 m^2. Robotic total station or RTK GPS surveys of wadable gravel beds with complex geometries are cost-effective for densities as high as ~2 pts per m^2. LIDAR remains problematic due to the biohazard of electromagnetic frequencies and amplitudes capable of penetrating water to sufficient depths clouded by sediment and bubbles. Boat-based echo sounder surveys yield extremely high resolution along boat transects, but also result in large gaps between transects. Tighter transects and future application of multi-beam sonar for shallow streams may eventually provide progress towards solving the problem, and thus have the most promise for solving this fundamental problem with 2D model application.

Even though there is error in 2D model predictions, there is also substantial error in field measurements. Velocity measurement involves a sensor-size trade-off. Sensors that function at the 1-10 cm scale may not resolve all theoretical factors impacting vertical-velocity pattern, but

Accepted

appear to accurately measure depth-averaged velocity. With substantial effort they can map cross-channel velocity patterns. Conversely, those that function at the 0.1-10 mm scale may distinguish skin friction from form drag, but do so at the cost of high sensitivity to even more complex micro-scale flow patterns that cannot be addressed theoretically. This level of detail would not be cost-effective as a tool for spatial flow mapping for 2D model validation in river management applications. Meanwhile, shear velocity may be estimated using many different equations involving various field measurements. Resulting values typically differ by ~50-70%. The error in 2D model predictions of shear velocity were within the 95% confidence limits of estimates based on field measurement ~60% of the time.

Given the errors reported above, it remains to be determined whether the 2D model application in this case is "validated" in light of the resultant numbers. Even though computational models solving the 2D St. Venant equations have been published, evaluated, and available for over 30 years, their increasing usage in scientific evaluation and societal management of complex river phenomena spanning hydrology, geomorphology, and ecology has re-raised the issue of model validation among a broader community. It is necessary to re-evaluate model assumptions for usage within the new settings they are being used as well as to validate model predictions for new functions that are extrapolated from model results through analytical, semi-analytical, or empirical relations. However, exactly what amount of error constitutes "validation" is unsettled in hydrology. Some rainfall-runoff studies as well as hydraulic studies use spatial or temporal pattern mimicry as sufficient validation, rarely presenting direct predicted versus observed plots and error estimates. This situation translates into confusion and conflict in the management arena.

At a minimum, when model predictions are within the range of error obtained in direct

Accepted

measurement or estimation based on measurement, then a model is at least as valid as measurement. This is the case with the 2D model shear velocity predictions made in this study. Despite the propagation of DEM errors through the model, the final predictions were accurate, except in very shallow locations close to the model threshold for drying. Thus, the 2D model is validated with respect to shear velocity. The magnitude of bed shear velocity predicted by the 2D model overestimates that obtained using near-bed velocity measurements by a factor of 2. Usage of this correction coefficient provides a simple and functional solution to the problem.

Validation of depth and velocity predictions depends on choosing a threshold level of error that is acceptable, and no universal threshold is identifiable. The threshold will depend on the purpose of the predictions and the associated level of accuracy needed. A finding from this study is that as much as 25% error in depth and 35% error in velocity prediction does not adversely affect shear velocity prediction enough to distinguish it from field-based estimation. Such thresholds will need to be determined for each new variable of interest as 2D model usage is expanded to address complex hydraulic-ecologic-geomorphic problems facing society.

Finally, it does appear that 2D depth, velocity, and shear velocity predictions were sufficiently accurate to conclude that 2D models can be an effective tool aiding river rehabilitation design and pre- or post- project appraisal. Aquatic ecologists sought to include significant habitat heterogeneity in the rehabilitation project to reflect their occurrence in undisturbed reference reaches. Neither steady, uniform flow equations (empirical or analytical) nor 1D computation models could resolve such 3D features. The 2D model could and did so successfully at the scale of 3-100 m. Where the 2D model did not perform well, was in resolving 0.1-1 m features that were inadequately mapped. At the scales where topographic features were resolved, post-project conditions were close to those predicted in the SHIRA design process,

Accepted

with most deviation due to the challenge of building the design using a rubber-tire front loader with limited depth capability. When viewed as one tool with its own limits and uncertainties among many such tools within a framework for site evaluation, a 2D model can shed significant insight into post-project conditions and help avoid costly mistakes.

ACKNOWLEDGEMENTS

Financial support for this work was provided by the US Fish and Wildlife Service (contracting entity for CALFED Bay-Delta Ecosystem Restoration Program: Cooperative Agreement DCN# 113322G003). The authors gratefully acknowledge EBMUD, Joe Merz, Jim Smith, Ellen Mantalica, Diana Cummings Brett Vallé, and Steven Winter for fieldwork assistance, helpful advice, administrative support, and equipment provision.

REFERENCES

Bates, P.D., Anderson, M.G. 1996. A preliminary investigation into the impact of initial conditions on flood inundationpredictions using a time/space distributed sensitivity analysis. *Catena* **26**, pp.115-134.

Bates, P.D., De Roo, A.P.J. 2000. A simple raster-based model for floodplain inundation. *Journal of Hydrology* **236**, pp. 54-77.

Bates, P.D., Anderson, M.G., Baird, L., Walling, D.E., Simm, D. 1992. Modelling floodplain flows using a two-dimensional finite element model. *Earth Surface Processes and Landforms* **17**, pp. 575–588.

Biron, P.M., Lane, S.N., Roy, A.G., Bradbrook, K.F., Richards, K.S., 1998, Sensitivity of Bed Shear velocity Estimated from Vertical Velocity Profiles: The Problem of Sampling Resolution. *Earth Surface Processes and Landforms* **23**, pp. 133-139.

Booker, D.J., Sear, D.A., Payne, A.J. 2001. Modelling three-dimensional flow structures and

Accepted

patterns of boundary shear velocity in a natural pool–riffle sequence. *Earth Surface Processes and Landforms* **26,** pp. 553–576.

Brasington, J., Rumsby, B.T., Mcvey, R.A. (2000). "Monitoring and modelling morphological change in a braided gravel-bed river using high resolution GPS-based survey", *Earth Surface Processes and Landforms* **25** 9, pp. 973–990.

Brown, L.R. 2000. Fish communities and their associations with environmental variables, lower San Joaquin River drainage, California. *Environmental Biology of Fishes* **57**, pp. 251–269.

Byrd, T.C., Furbish, D.J. 2000. Magnitude Of Deviatoric Terms In Vertically Averaged Flow Equations. *Earth Surface Process and Landforms* **25**, pp. 319-328.

Cao, Z., Carling, P., Oakley, R. 2003. Flow reversal over a natural pool-riffle sequence: a computational study. *Earth Surface Processes and Landforms* **28,** pp. 689-705.

Fisher, F. 1994. Past and present status of Central Valley chinook salmon. *Conservation Biology* **8** 3, pp. 870-873.

French, J.R., Clifford, N.J. 2000. Hydrodynamic modeling as a basis for explaining estuarine environmental dynamics: some computational and methodological issues. *Hydrological Processes* **14**, pp. 2089-2108.

Froehlich, D.C. 1989. Finite element surface-water modeling system: two-dimensional flow in a orizontal plane user's manual. *U.S. Department of Transportation, Publication #FHWA-RD-88-177*, 285 pp.

Gard, M. 2003. Flow-habitat relationships for spring-run Chinook salmon spawning in Butte Creek. *United States Fish and Wildlife Service, Energy Planning and Instream Flow Branch*, Sacramento, CA, 86 pp.

Gard, M. 2005. Monitoring of restoration projects in the Merced River using 2-dimensional modelling methodology. *United States Fish and Wildlife Service, Energy Planning and Instream Flow Branch,* Sacramento, CA, 86 pp.

Ghanem, A, Steffler, P, Hicks, F. 1996. Two-dimensional hydraulic simulation of physical habitat conditions in flowing streams. *Regulated Rivers: Research & Management* **12**, pp. 185-200.

Hardy, R.J., Bates, P.D., Anderson, M.G. 1999. The importance of spatial resolution in hydraulic models for floodplain environments. *Journal of Hydrology* **216**, pp. 124–136

Lane, S.N., and Richards, K.S. 1998. High resolution, two-dimensional spatial modelling of flow processes in a multi-thread channel. *Hydrological Processes* **12**, pp. 1279-1298.

Lane, S.N., Bradbrook, K.F., Richards, K.S., Biron, P.M., Roy, A.G. 1999. The application of

Accepted

computational fluid dynamics to natural river channels: three-dimensional versus two-dimensional approaches. *Geomorphology* **29**, pp. 1-20.

Lawless, M., Robert, A., 2001, Scales of Boundary Resistance in Coarse-grained Channels: Turbulent Velocity Profiles and Implications. *Geomorphology* **39**, pp. 221-238.

Leclerc, M., Boudreault, A., Bechara, J.A., Corfa, G. 1995. Two-dimensional hydrodynamic modeling: a neglected tool in the instream flow incremental methodology. *Transactions of the American Fisheries Society* **124**, pp. 645-662.

McCuen, RH. 1989. *Hydrologic Analysis and Design*. Prentice Hall: Englewood Cliffs.

Merz, J.E., L.K. Ochikubo Chan. 2005. Effects of gravel augmentation on macroinvertebrate assemblages in a regulated California river. *River Research and Applications* **21**, pp. 61-74.

Merz, J.E., J.D. Setka. 2004. Evaluation of a spawning habitat enhancement site for chinook salmon in a regulated California river. *North American Journal of Fis heries Management* **24**, pp. 397-407.

Merz, J.E., Pasternack, G.B., Wheaton, J.M. In Press. Sediment Budget for Salmonid Spawning Habitat Rehabilitation in the Mokelumne River. Geomorphology.

Merz, J.E., Setka, J., Pasternack, G.B., Wheaton, J.M. 2004. Predicting benefits of spawning habitat rehabilitation to salmonid fry production in a regulated California river. Canadian *Journal of Fisheries and Aquatic Science* **61**, pp. 1433-1446.

Miller, A.J. 1995. Valley morphology and boundary conditions influencing spatial patterns of flood flow. In *Natural and Anthropogenic Influences in Fluvial Geomorphology*, Costa JE, Miller AJ, Potter KW, Wilcock PR (eds). American Geophysical Union: Washington, DC, pp. 57-81.

Miller, A.J., Cluer B.L. 1998. Modeling considerations for simulation of flow in bedrock channels. In *Rivers Over Rock: Fluvial Processes in Bedrock Channels*, Wohl EE, Tinkler KJ (eds). American Geophysical Union: Washington, DC, pp. 61-104.

Moulin, C., Ben Slama, E. 1998. The two-dimensional transport module SUBIEF. Applications to sediment transport and water quality processes. *Hydrological Processes* **12**, pp. 1183-1195.

Moyle, P.B. 1994. The decline of anadromous fishes in California. *Conservation Biology* **8** 3, pp. 869-870.

Moyle, P.B., Randall, P.J. 1998. Evaluating the biotic integrity of watersheds in the Sierra Nevada, California. *Conservation Biology* **12,** pp. 1318-1326.

Nelson, J.M., Schmeeckle, M. W., Shreve, R.L. 2001. Turbulence and Particle Entrainment. In

Accepted

Gravel-Bed Rivers V, Mosley, M.P. (ed). New Zealand Hydrological Society, p. 221-248.

Nicholas, A.P., Sambrook Smith, G.H. 1999. Numerical simulation of three-dimensional flow hydraulics in a braided channel. *Hydrological Processes* **13**, pp. 913-929.

Nicholas, A.P., Walling, D.E. 1998. Numerical modelling of floodplain hydraulics and suspended sediment transport and deposition. *Hydrological Processes* **12**, pp. 1339-1355.

Pasternack, G.B., Wang, C.L., Merz, J.E. 2004. Application of a 2D hydrodynamic model to reach-scale spawning gravel replenishment on the lower Mokelumne River, California. *River Research and Applications* **20** 2, pp. 205-225.

Rathburn, S.L. 2001. Modeling pool sediment dynamics in a mountain river. Colorado State University, PhD Thesis, 204 pp.

Rathburn, S.L., Wohl, E.E. 2003. Predicting fine sediment dynamics along a pool-riffle mountain channel, *Geomorphology* **55** 1-4, pp. 111-124.

Rhoades, B.L., Kenworthy, S.T. 1995. Flow structure at an asymmetrical stream confluence. *Geomorphology* **11** 4, pp. 273-293.

Robert, A. 1997. Characteristics of velocity profiles along riffle-pool sequences and estimates of bed shear velocity. *Geomorphology* **19,** pp. 89-98.

Shields, F.D. Knight, S.S., Testa, S., Cooper, C.M. 2003. Use of Acoustic Doppler Current Profilers to Describe Velocity Distributions at the Reach Scale. *Journal of the American Water Resources Association* **39** 6, pp. 1397-1408.

Shuman, J.R. 1995. Environmental considerations for assessing dam removal alternatives for river restoration. *Regulated Rivers: research and management* **11**, pp. 249-261.

Smart, G.M., 1999, Turbulent Velocity Profiles and Boundary Shear in Gravel Bed Rivers. *Journal of Hydraulic Engineering* **125**, pp. 106-116.

Stewart, M. D., Bates, P. D., Price, D. A., Burt, T. P. 1998. Modelling the spatial variability in floodplain soil contamination during flood events to improve chemical mass balance estimates. *Hydrological Processes* **12**, pp. 1233-1255.

Stewart, M.D. Bates, P.D., Anderson, M.G. Price, D.A. Burt, T.P. 1999. Modelling floods in hydrologically complex lowland river reaches. *Journal of Hydrology* **223**, pp. 85–106.

Tchamen, G.W., Kahawita, R.A. 1998. Modelling wetting and drying effects over complex topography. *Hydrological Processes* **12**, pp. 1151-1182.

Tiffan, K.F., Garland, R.D., Rondorf, D.W. 2002. Quantifying Flow-Dependent Changes in Subyearling Fall Chinook Salmon Rearing Habitat Using Two-Dimensional Spatially

Accepted

Explicit Modeling. *North American Journal of Fisheries Management* **22,** pp. 713–726.

Wheaton, J.M., Pasternack, G.B., Merz, J.E. 2004 A. Spawning Habitat Rehabilitation - 1. Conceptual Approach & Methods. *Journal of River Basin Management.* **2**, pp. 3-20.

Wheaton, J.M., Pasternack, G.B., Merz, J.E. 2004 B. Spawning Habitat Rehabilitation - 2. Using hypothesis development and testing in design, Mokelumne River, California, U.S.A. *Journal of River Basin Management.* **2**, pp. 21-37.

Wheaton, J.M., Pasternack, G.B., Merz, J.E. 2004 C. Use of habitat heterogeneity in salmonid spawning habitat rehabilitation design. in Fifth International Symposium on Ecohydraulics: Aquatic Habitats: Anlalysis and Restoration, IAHR-AIRH: Madrid, Spain. p. 791-796.

Wiberg, P.L., Smith, J.D., 1991, Velocity Distribution and Bed Roughness in High-Gradient Streams. *Water Resources Research* **27**, pp. 825-838.

Wilcock, P.R., 1996, Estimating Bed Shear velocity from Velocity Observations. *Water Resources Research* **32,** pp. 3361-3366.

Accepted

Figure Captions

Figure 1. Study site maps. A) Mokelumne River basin map; B) topographic map of model domain showing gravel placement area as well as 2 cross-sections and 6x4 tracer-core locations.

Figure 2. Photo of installed tracer cores at location 1 illustrating size classes of cores and the size distribution of surrounding artificially placed coarse sediment.

Figure 3. Vertical velocity profiles over 23 tracer cores organized by location and size class.

Figure 4. Post-project 2D model hydrodynamic predictions for the 2002 rehabilitation site at 7.25 cumecs. Shading corresponds to depth solutions and arrows correspond to velocity vectors (scaled to magnitude). Vector density reflects computation mesh resolution. Ovals with circles inside are tracer core locations.

Figure 5. Comparisons of observed versus predicted depths and velocities at cross-sections 4 (a,b) and 7 (c,d). Field observations were fit with a curve using the locally weighted Least Squared error method to reduce measurement noise.

Figure 6. Observed versus predicted depths at 23 tracer-core locations showing the largest errors near the wet-dry boundary and where the DEM was faulty.

Figure 7. Assessment of velocity predictions at 23 tracer-core locations. A) observed versus predicted depths and B) analysis showing that depth error was the primary cause of error in velocity prediction (outliers have X-symbols).

Figure 8. Comparison of u* estimation methods using field-measured depth-averaged velocity and either eq. (4) with a global z_o (open symbols) or eqs. (1,2) (closed symbols).

Figure 9. Estimated versus 2D-model predicted u* based on eqs. (1,2) with depth-averaged

Accepted

velocity (filled symbols) and based on eq. (4) using a global z_o (open symbols). Solid line is 1:1 while dashed lines are 95% confidence limits on open symbol estimates.

Figure 10. Analysis showing that velocity error was the predominant cause of error in u* prediction (outlier has an X-symbol).

Figure 11. Analysis showing that the velocity gradient of the whole vertical velocity profile was the primary cause of the difference between total and near-bed u*.

Accepted